Kinetics and structural features of dimeric glutamine-dependent bacterial NAD$^+$ synthetases suggest evolutionary adaptation to available metabolites

Received for publication, February 2, 2018, and in revised form, March 11, 2018 Published, Papers in Press, March 26, 2018, DOI 10.1074/jbc.RA118.002241

Adrian Richard Schenberger Santos[‡], Edileusa Cristina Marques Gerhardt[‡], Vivian Rotuno Moure[‡], Fábio Oliveira Pedrosa[‡], Emanuel Maltempi Souza[‡], Riccardo Diamanti[§], Martin Högbom[§], and Luciano Fernandes Huergo[‡¶1]

From the [‡]Department of Biochemistry and Molecular Biology and [¶]Setor Litoral, Universidade Federal do Paraná (UFPR), Curitiba, PR, 512 Brazil and the [§]Department of Biochemistry and Biophysics, Stockholm University, 106 91 Stockholm, Sweden

Edited by John M. Denu

NADH (NAD$^+$) and its reduced form NADH serve as cofactors for a variety of oxidoreductases that participate in many metabolic pathways. NAD$^+$ also is used as substrate by ADP-ribosyl transferases and by sirtuins. NAD$^+$ biosynthesis is one of the most fundamental biochemical pathways in nature, and the ubiquitous NAD$^+$ synthetase (NadE) catalyzes the final step in this biosynthetic route. Two different classes of NadE have been described to date: dimeric single-domain ammonium-dependent NadE^{NH3} and octameric glutamine-dependent NadE^{Gln}, and the presence of multiple NadE isoforms is relatively common in prokaryotes. Here, we identified a novel dimeric group of NadE^{Gln} in bacteria. Substrate preferences and structural analyses suggested that dimeric NadE^{Gln} enzymes may constitute evolutionary intermediates between dimeric NadE^{NH3} and octameric NadE^{Gln}. The characterization of additional NadE isoforms in the diazotrophic bacterium *Azospirillum brasilense* along with the determination of intracellular glutamine levels in response to an ammonium shock led us to propose a model in which these different NadE isoforms became active accordingly to the availability of nitrogen. These data may explain the selective pressures that support the coexistence of multiple isoforms of NadE in some prokaryotes.

NADH (NAD$^+$) and its reduced form NADH serve as cofactors for a variety of oxidoreductases that participate in a diverse range of metabolic pathways. More recently, NAD$^+$ has also been implicated in signal transduction mechanisms. Studies in mammals showed that a conserved Nudix domain NAD$^+$ sensor protein regulates DNA repair mechanisms, thereby relating NAD$^+$ levels to cancer and aging (1). NAD$^+$ is also used as substrate for signaling pathways by mono- and poly-ADP-ribosyl-transferases and by sirtuins (2–4). Furthermore, manipulation of the NAD$^+$/NADH levels in microorganisms can help to develop or improve a plethora of biotechnological processes.

NAD$^+$ biosynthesis is a fundamental biochemical process in all cells, it can occur *de novo* or through salvage pathways. The last reaction step in *de novo* pathway and in some of the NAD$^+$ salvage pathways is the amidation of nicotinic acid adenine dinucleotide (NaAD)[2] to form NAD$^+$, a reaction catalyzed by the ubiquitous NAD$^+$ synthetase (NadE) (5). In the first reaction step, NadE uses NaAD and ATP as substrates, forms a NaAD-AMP intermediate (thereby activating the carboxyl group of nicotinamide) and releases PP_i. In the second reaction step, NH_3 acts as a nucleophile to attack NaAD-AMP releasing NAD$^+$ and AMP as final products (6).

Two different classes of NadE are found in nature. Single domain ammonium-dependent NadE^{NH3} (EC 6.3.1.5) is present in Bacteria and Archaea and uses external ammonium as the N donor. These enzymes are homodimers and have been extensively characterized biochemically and structurally (7–9). The second class is the glutamine-dependent NadE^{Gln} (EC 6.3.5.1) which is present in Eukarya, Bacteria, and Archaea and is able to use L-glutamine as N donor because of the presence of an extra N-terminal glutaminase domain (CN hydrolase domain) (9). Just a few NadE^{Gln} have been characterized in prokaryotes (10–12).

The best studied NadE^{Gln} is from *Mycobacterium tuberculosis* (MtNadE^{Gln}), this enzyme is arranged as a homooctamer where the N-terminal glutaminase domain from one subunit connects with the C-terminal synthetase domain from another subunit. The ammonia released from glutamine hydrolysis is directed to the synthetase domain through a 40 Å intersubunit ammonia tunnel (13). The MtNadE^{Gln} exhibits strong synergism between the two catalytic domains such that efficient glutamine hydrolysis only occurs in the presence of NaAD and ATP and depends of the formation of the NaAD-AMP intermediate. Conversely, the presence of glutamine significantly decreases the K_m for NaAD and ATP.

Extensive genomic context analysis revealed that a few prokaryotic single-domain NadE (presumably NadE^{NH3} as judged by domain organization) are actually clustered with a separate

This work was supported by Conselho Nacional de Desenvolvimento Científico e Tecnológico (CNPq), Fundação Araucária, Coordenação de Aperfeiçoamento de Pessoal de Ensino Superior (CAPES), and CNPq-Instituto Nacional de Ciência e Tecnologia (INCT). The authors declare that they have no conflicts of interest with the contents of this article.

This article contains Table S1 and Figs. S1–S5.

[1] To whom correspondence should be addressed: Setor Litoral, UFPR, Matinhos, PR, Rua Jaguariaíva, 512 Brazil. Tel.: 55-41-33611570; Fax: 55-41-33161570; E-mail: luciano.huergo@gmail.com.

[2] The abbreviations used are: NaAD, nicotinic acid adenine dinucleotide; PDB, Protein Data Bank.

gene encoding a glutaminase and, at least in the case of *Thermus thermophilus*, these domains can interact to form a holoenzyme that is able to utilize glutamine to direct NAD^+ formation *in vitro* (9). Based on these studies, an evolutionary scenario has been postulated where a single-domain $NadE^{NH3}$ was present in last universal common ancestor (LUCA), and the two-domain $NadE^{Gln}$ evolved via recruitment and fusion of the N-terminal glutaminase domain (9).

Genome analysis revealed that some prokaryotes can encode up to three different NadE (9). Two different genes encoding two-domain $NadE^{Gln}$ have been identified in the diazotrophic endophytic β-Proteobacterium *Herbaspirillum seropedicae*. In a previous study we presented the biochemical characterization of $HsNadE1^{Gln}$, which resembled the properties of the archetypical $NadE^{Gln}$ from *M. tuberculosis*; it is also arranged as a homo-octamer and preferentially uses glutamine and N donor (12).

Here we describe the biochemical characterization of the second $NadE^{Gln}$ from *H. seropedicae* (named $NadE2^{Gln}$). Surprisingly, we observed that $HsNadE2^{Gln}$ forms a lower oligomeric structure (probably a homodimer) and can use both ammonium and glutamine as N donor.

From now on we will use the term $NadE^{NH3}$ to describe single-domain homodimeric enzymes. $NadE^{Gln}$ will be used to describe enzymes carrying the additional N-terminal glutaminase domain with numbers 1 and 2, indicating quaternary structures arranged as octamers or dimers, respectively.

Oligomerization studies of the two $NadE^{Gln}$ detected in the diazotrophic α-Proteobacterium *Azospirillum brasilense* also showed that $AbNadE1^{Gln}$ forms an octamer, whereas $AbNadE2^{Gln}$ is a dimer. Furthermore, PDB searches identified two structures of dimeric $NadE2^{Gln}$: one in the β-Proteobacterium *Burkholderia thailandensis* (PDB code 4F4H) and the other in the δ-Proteobacterium *Acinetobacter baumannii* (PDB code 5KHA). Phylogenetic analysis showed that all these dimeric $NadE2^{Gln}$ form a separate group distinct from the octameric $NadE1^{Gln}$. Structural comparisons between dimeric *A. baumannii* and octameric $MtNadE1^{Gln}$ show that the dimeric and octameric proteins possess similar domain interaction geometry between the glutaminase and synthetase domains achieved through an interprotein domain swapping in the octameric enzymes. In addition to the substrate-binding sites, a conserved intersubunit ammonia tunnel could be detected. We speculate that dimeric $NadE2^{Gln}$ are evolutionary intermediates between single-domain dimeric $NadE^{NH3}$ and two-domain octameric $NadE1^{Gln}$.

Results

Characterization of H. seropedicae $NadE2^{Gln}$ (HsNadE2)

A previous report indicated the presence of two putative glutamine-depended NAD^+ synthetase encoded by the genome of *H. seropedicae.* One of these enzymes, namely $HsNadE1^{Gln}$, has been characterized previously, and its oligomerization and biochemical properties resemble the characteristics of $MtNadE1^{Gln}$ (12). The second glutamine-dependent NadE from *H. seropedicae* (Uniprot D81X05), namely $HsNadE^{Gln}$, has the two domains typically present in other types of $NadE^{Gln}$ according to Pfam: an N-terminal glutaminase domain (CN hydrolase, amino acids 3–252) and a C-terminal NAD synthase domain (amino acids 281–542). Sequence alignments with other characterized $NadE^{Gln}$ showed that $HsNadE2^{Gln}$ carries the conserved glutamine catalytic triad EKC in the N-terminal region and the conserved residues involved in NaAD and ATP binding in the C-terminal region (Fig. 1).

The gene encoding $HsNadE2^{Gln}$ was cloned into pET28a, and the protein was expressed as a N-terminal His_6 tag fusion protein using *Escherichia coli* BL21 (λDE3) as host. $HsNadE2^{Gln}$ was purified by Ni^{2+}-affinity chromatography. Analytical gel filtration was performed, and $HsNadE2^{Gln}$ eluted as a single homogeneous peak with the elution volume corresponding to 85 kDa (Figs. S1 and S2). Because the calculated mass for each monomer is 61 kDa, the gel-filtration analysis supports that HsNadE2 is arranged in a different oligomeric state, contrasting with the octameric $MtNadE1^{Gln}$ and $HsNadE1^{Gln}$.

The activity of $HsNadE2^{Gln}$ was determined by coupling NAD^+ formation with the activity of alcohol dehydrogenase and following the absorbance of NADH at 340 nm. The substrates NaAD and ATP were kept at saturating levels, and the experiments were performed with increasing concentrations of ammonium or glutamine to determine kinetic parameters for these two substrates. For both ammonium and glutamine the initial velocity *versus* substrate concentration exhibited typical Michaelis–Menten hyperbolic response (Fig. S2). The determined K_m for ammonium and glutamine were in the same order of magnitude, being 240 and 130 μM, respectively (Table 1). This is in contrast $MtNadE1^{Gln}$ and $HsNadE1^{Gln}$, which have a K_m for glutamine at least 1 order of magnitude lower that for ammonium (Table 1). The K_m values of $HsNadE2^{Gln}$ are more related to the values obtained for a $NadE^{Gln}$ characterized in the deep-branching Bacteria *Thermotoga maritima* (Table 1). Note that no information about the oligomerization state is available for $TmNadE^{Gln}$. Comparison of the k_{cat}/K_m values, which are indicative of substrate preference, showed that $HsNadE2^{Gln}$ and $TmNadE^{Gln}$ have no significant preference N donor substrates. On the other hand, $HsNadE1^{Gln}$ and $MtNadE1^{Gln}$ showed a clear preference to use glutamine as N donor (Table 1).

The preference for the utilization of ammonium or glutamine was compared between $HsNadE1^{Gln}$ and $HsNadE2^{Gln}$ using LC/MS. For this analysis, unlabeled glutamine is mixed with $^{15}NH_4Cl$, and the ratio of ^{15}N NAD^+ and ^{14}N NAD^+ (NH_4^+/Gln) formed is determined using LC coupled to high resolution MS. The results confirmed that $HsNadE1^{Gln}$ has a stronger preference for glutamine than $HsNadE2^{Gln}$ (Table 2). When both ammonium and glutamine were available at equimolar concentration (2 mM), $HsNadE2^{Gln}$ was able to incorporated 11.9-fold more ammonium in relation to glutamine than $HsNadE1^{Gln}$ (Table 2).

Characterization of the three NadE from A. brasilense

An inspection on the genome of the diazotrophic plant associative α-Proteobacterium *A. brasilense* Sp245 revealed the presence of three NadE-like genes: first a single-domain $NadE^{NH3}$ type (Uniprot G8ATC0), namely $AbNadE^{NH3}$, and the other two belonging to the $NadE^{Gln}$ type, namely

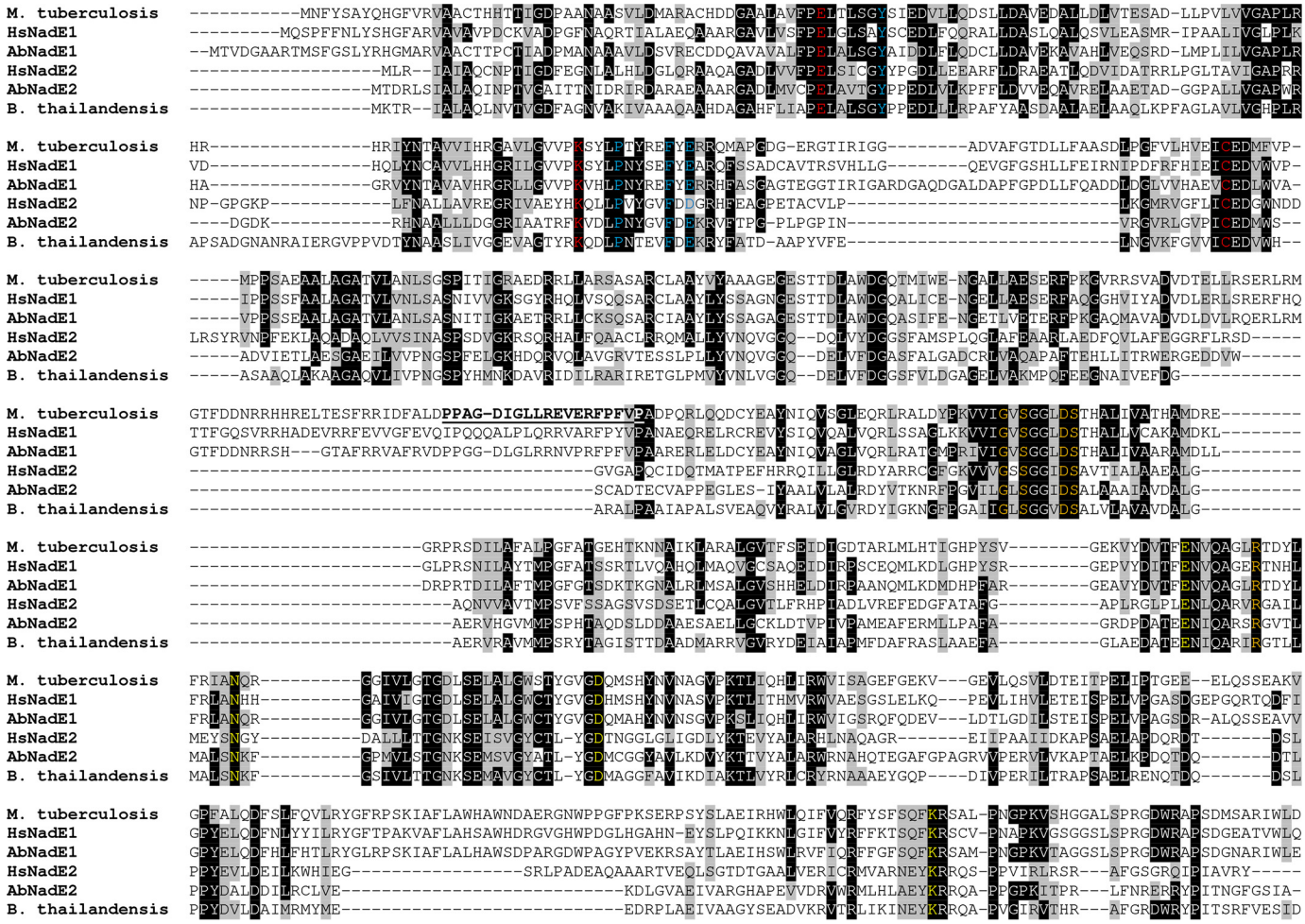

Figure 1. Sequence alignment of different NadE^{Gln}. The sequences of *M. tuberculosis*, *H. seropedicae* NadE1^{Gln} and NadE2^{Gln}, *A. brasilense* NadE1^{Gln} and NadE2^{Gln}, and *B. thailandensis* were aligned using Clustal W. The threshold for shading was set as 60%. The conserved catalytic triad EKC present in the glutaminase domain is indicated in *red*. Conserved residues involved in NaAD and ATP binding are indicated in *yellow* and *orange*, respectively. Residues forming the ammonia tunnel constriction are indicated in *blue*. The interdomain loop in MtNadE1^{Gln} is *underlined*.

Table 1

Kinetic properties in different Gln-dependent NadE

Organism	Substrate	K_m	k_{cat}	k_{cat}/K_m	Preference	Reference
		mM	s^{-1}	s^{-1}/mM		
M. tuberculosis	NH_4^+	20 ± 2	3.0 ± 0.1	0.15 ± 0.02	2.8	Ref. 13
MtNadE1	Gln	1.3 ± 0.1	0.55 ± 0.01	0.42 ± 0.03	Gln > NH_4^+	
T. maritima	NH_4^+	0.33 ± 0.1	0.24 ± 0.04	0.7 ± 0.3	0.9	Ref. 11
	Gln	0.42 ± 0.05	0.29 ± 0.01	0.68 ± 0.08	NH_4^+ > Gln	
T. thermophilus	NH_4^+	0.03 ± 0.01	0.09 ± 0.03	3	50	Ref. 9
	Gln	0.73 ± 0.19	0.04 ± 0.01	0.06	NH_4^+ > Gln	
HsNadE1	NH_4^+	5.7 ± 0.61	0.05 ± 0.001	0.009 ± 0.0001	9	Ref. 12
	Gln	0.37 ± 0.08	0.03 ± 0.02	0.08 ± 0.02	Gln > NH_4^+	
HsNadE2	NH_4^+	0.24 ± 0.07	0.07 ± 0.01	0.29 ± 0.08	2.4	This work
	Gln	0.13 ± 0.02	0.09 ± 0.01	0.69 ± 0.05	Gln > NH_4^+	
AbNadE1	NH_4^+	10.01 ± 0.84	0.23 ± 0.01	0.02 ± 0.001	140	This work
	Gln	0.08 ± 0.005	0.23 ± 0.003	2.8 ± 0.23	Gln > NH_4^+	
AbNadE2	NH_4^+	1.85 ± 0.13	0.06 ± 0.004	0.03 ± 0.001	1.6	This work
	Gln	0.82 ± 0.08	0.04 ± 0.001	0.05 ± 0.006	Gln > NH_4^+	

AbNadE1^{Gln} (Uniprot G8AIW8) and AbNadE2^{Gln} (Uniprot G8ATT3). The genes encoding these proteins were cloned and expressed as recombinant proteins in *E. coli* BL21 (λDE3). The proteins were purified to homogeneity as judged by SDS-PAGE (Fig. S3).

Analytical gel filtration revealed that all three NadE eluted as a homogeneous symmetric peak with elution volumes

Table 2

Ammonium *versus* glutamine competition in *H. seropedicae* NadE1 and NadE2

Substrate concentrations	HsNadE1 NH_4^+/Gln	HsNadE2 NH_4^+/Gln	HsNadE2/ HsNadE1 ratio
2 mM glutamine and 0.2 mM NH_4Cl	0.05	0.34	6.8
0.2 mM glutamine and 2 mM NH_4Cl	0.18	5.26	29.2
2 mM glutamine and 2 mM NH_4Cl	0.15	1.78	11.9

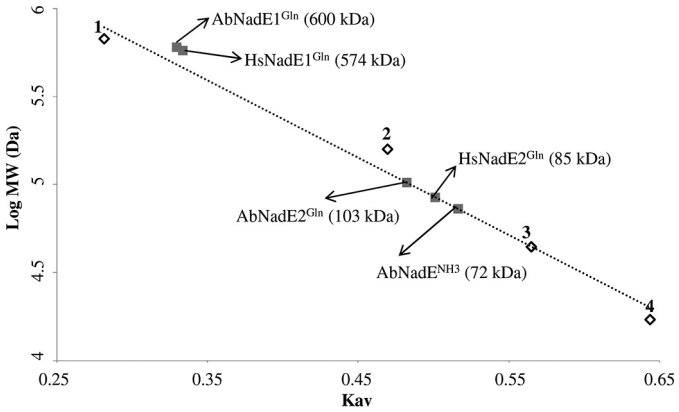

Figure 2. Gel filtration analysis of the different NadE. Gel filtration was performed on a Superose 6 column (GE Healthcare), which was calibrated with a range of molecular mass standards (Bio-Rad): *point 1*, thyroglobulin; *point 2*, bovine γ-globulin; *point 3*, chicken ovalbumin; and *point 4*, equine myoglobin. The *arrows* indicate the estimated molecular weight of each NadE protein.

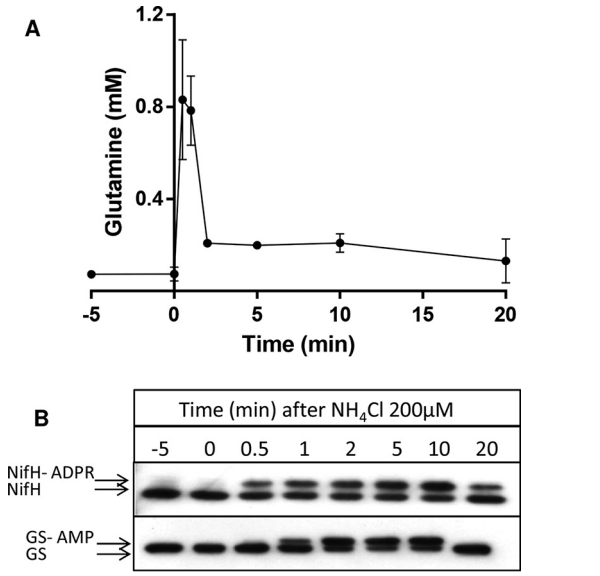

Figure 3. Intracellular levels of glutamine and NifH and GS modification after an ammonium shock in *A. brasilense*. *A*, average intracellular glutamine levels from triplicate experiments ± S.D. *B*, Western blotting analysis showing of the reversible post-translational modification of NifH and GS. The *upper bands* represent the ADP-ribosylated NifH (NifH-ADPR) or adenylylated GS (GS-AMP).

corresponding to 600, 103, and 72 kDa for AbNadE1^{Gln}, AbNadE2^{Gln}, and AbNadE^{NH3}, respectively (Fig. 2 and Fig. S4). The determined molecular weight fits with dimer oligomerization for AbNadE2^{Gln} and AbNadE^{NH3} (calculated masses are 120 kDa for dimer AbNadE2 and 74 kDa for AbNadE3). On the other hand, AbNadE1^{Gln} is arranged as an octamer (calculated mass for octamer is 605 kDa); hence AbNadE1^{Gln} resembles the oligomeric organization found in HsNadE1^{Gln} and MtNadE1^{Gln} (all octameric).

The AbNadE^{NH3} belongs to the NadE^{NH3} type and showed a dimeric organization. As expected, AbNadE^{NH3} was not able to use glutamine as N donor for NAD^+ production (data not shown). On the other hand, the identification of a dimeric NadE^{Gln} also in *A. brasilense* supports the presence of a novel subgroup of NadE^{Gln}, which is different from the archetypical octameric NadE^{Gln} described in *M. tuberculosis* and eukaryotes such as *Saccharomyces cerevisiae*.

The kinetic characterization of the two *A. brasilense* NadE^{Gln} revealed the same trend as observed for the *H. seropedicae* enzymes. The dimeric AbNadE2^{Gln} showed a K_m for ammonium and glutamine in the same order of magnitude being 1,850 and 820 μM, respectively (Table 1). On the other hand, the octameric AbNadE1^{Gln} had a K_m for glutamine more than 2 orders of magnitude lower that for ammonium (Table 1). The k_{cat}/K_m values clearly show that AbNadE1^{Gln} has a strong preference for glutamine as N donor, whereas AbNadE2^{Gln} can use both substrates with nearly similar preference (Table 1).

Intracellular glutamine levels in A. brasilense

It is well-established that the intracellular glutamine levels in Proteobacteria correlates with the availability of ammonium in the culture media (14, 15). Particularly, in some nitrogen fixing organisms, such as *A. brasilense* and *H. seropedicae*, nitrogen fixation only occurs when the intracellular glutamine levels are low (16, 17).

We used untargeted LC/MS to determine the intracellular levels of glutamine in *A. brasilense*. Under nitrogen-fixing conditions, the glutamine levels ranged between 74 and 79 μM (Fig. 3*A*). After the addition of 200 μM of NH_4Cl to the cells, the intracellular levels of glutamine augmented to 830 μM in just 30 s and remained at similar levels after 1 min (Fig. 3*A*). 2 min after the ammonium shock, the ammonium added is consumed by the cellular metabolism, and the intracellular glutamine levels declined to 200 μM, decreasing even further after 20 min (Fig. 3*A*). These fluctuations in intracellular glutamine were well-synchronized with the covalent modification of the nitrogenase component NifH and glutamine synthetase GS (Fig. 3*B*). Both NifH and GS are known to suffer reversible covalent modification that inactivates both enzymes in response to an ammonium shock (18, 19).

Under nitrogen-fixing conditions, the intracellular levels of glutamine were nearly identical to the AbNadE1^{Gln} K_m for glutamine (~80 μM) and ~10-fold below the AbNadE2^{Gln} K_m for glutamine (Table 1 and Fig. 3*A*). These data suggest that AbNadE1^{Gln} is much more active than AbNadE2^{Gln} under nitrogen-fixing conditions. In contrast, upon an ammonium shock, the intracellular levels of glutamine reached the AbNadE2^{Gln} K_m for glutamine (~800 μM). Hence, upon an ammonium shock, AbNadE2^{Gln} should become more active, whereas AbNadE1^{Gln} should be operating at V_{max} (Fig. S2)

The LC/MS metabolome data were submitted to XCMS software (20) to identify other potential metabolites that fluctuate in response to the ammonium shock. However, only glutamine showed statistical significant fluctuations ($p < 0.05$). Even though other metabolites such as NADH, NAD^+, ATP, ADP, AMP, and 2-oxoglutarate could be detected in the analysis (as suggested by comparison of retention times and m/z to authenticated standards), their low signal and/or high variation among biological replicates did not allow their quantification.

Phylogeny analysis of dimeric NadE^{Gln}

The presence of other representatives of dimeric NadE2^{Gln} in nature is supported by at least two structures deposited in the

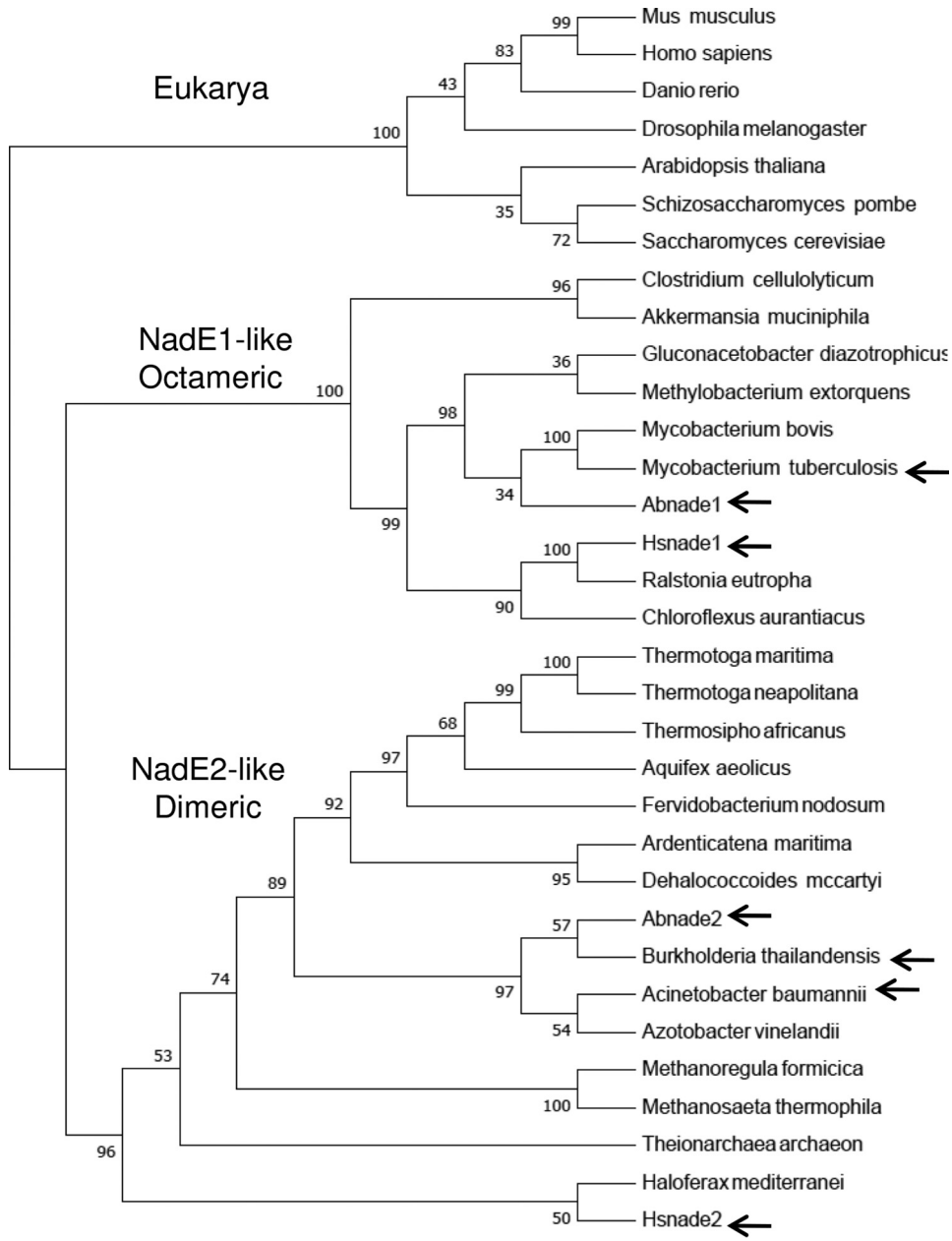

Figure 4. Phylogenetic analysis of selected NadE^{Gln}. The sequence of NadE^{Gln} was retrieved from NCBI and aligned using Clustal W. The phylogentic three was constructed by Neighbor-joining using MEGA 7. All positions containing gaps and missing data were eliminated from the data set. Bootstrap values were adjusted to 1000 replicates. Three groups were observed: 1) eukaryotic representatives; 2) NadE1-like octameric NadE^{Gln}; and 3) NadE2-like dimeric NadE^{Gln}. The relevant proteins with experimentally determined quaternary structure are indicated by *arrows*. *A. baumannii*, WP_065718975.1; *Akkermansia muciniphila* ATCC BAA-835, ACD04457.1; *Aquifex aeolicus*, NP_213654.1; *Arabidopsis thaliana*, NP_175906.1; *Ardenticatena maritima*, KPL88222.1; *A. brasilense*, AIB10872.1; *A. brasilense*, AIB14429.1; *Azotobacter vinelandii* DJ, YP_002798395.1; *B. thailandensis*, AOJ56104.1; *Chloroflexus aurantiacus*, ABY34602.1; *Clostridium cellulolyticum* H10, YP_002505537.1; *Danio rerio*, NP_001092723.1; *Dehalococcoides mccartyi* 195, YP_181837.1; *Drosophila melanogaster*, NP_572913.1; *Fervidobacterium nodosum* Rt17-B1, YP_001410277.1; *Gluconacetobacter diazotrophicus* PA1 5, YP_001601200.1; *Haloferax mediterranei*, AHZ23047.1; *H. seropedicae*, AKN65438.1; *H. seropedicae*, AKN67808.1; *Homo sapiens*, NP_060631.2; *Methanoregula formicica*, AGB01500.1; *Methanosaeta thermophila* PT, YP_843157.1; *Methylobacterium extorquens* CM4, YP_002423109.1; *Mus musculus*, NP_084497.1; *Mycobacterium bovis* AF2122/97, NP_856111.1; *Ralstonia eutropha* H16, YP_725265.1; *S. cerevisiae* S288C, NP_011941.1; *Schizosaccharomyces pombe* 972h-, NP_587771.1; *Theionarchaea archaeon*, KYK35595.1; *Thermosipho africanus* TCF52B, YP_002335497.1; *T. maritima*, AKE27162.1; *Thermotoga neapolitana* DSM 4359, YP_002534863.1; and *M. tuberculosis*, AMP30329.1.

PDB. The NadE2^{Gln} from the β-Proteobacterium *B. thailandensis* (PDB code 4F4H) and from the δ-Proteobacterium *A. baumannii* (PDB code 5KHA). A Neighbor-joining phylogenetic tree was constructed using the alignment of NadE^{Gln} sequences derived from organisms belonging to all domains of life (Fig. 4). The sequences were separated into three distinct groups; 1) the eukaryotic NadE1^{Gln}; 2) a group containing the octameric NadE1^{Gln} from *M. tuberculosis, H. seropedicae* and *A. brasilense*; and 3) a more diverse group comprising all the NadE2^{Gln} described as dimeric. This last group includes the sequences of deep branching Bacteria (Thermotoga and Aquifex) and Archaea (Fig. 4).

Structural analysis of dimeric NadE2^{Gln}

Given the availability of a 1.7 Å resolution structure of dimeric NadE2^{Gln} from *B. thailandensis* (PDB code 4F4H)

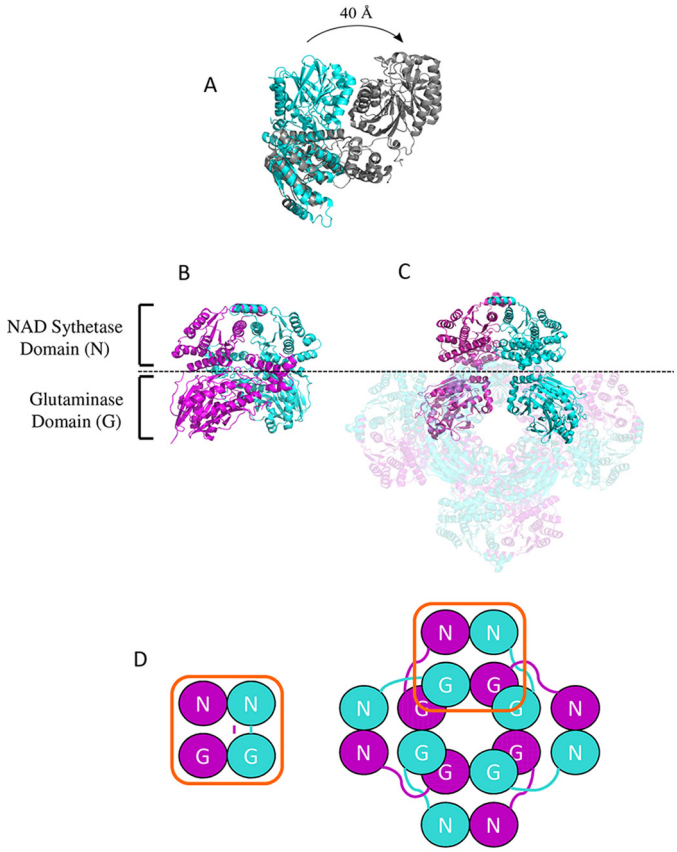

Figure 5. Comparison between the structures of dimeric and octameric NadE^{Gln}. *A*, superimposition of the single chain of NadE2^{Gln} from *B. thailandensis* (*cyan*) and NadE1^{Gln} from *M. tuberculosis* (*gray*). The PDB structures 4FH4 and 3DLA were superimposed using COOT and visualized using PyMOL. Structures are colored by chain. *B* and *C*, comparison between the organization of dimeric NadE^{Gln} from *B. thailandensis* (*B*) and octameric NadE^{Gln} from *M. tuberculosis* (*C*). Only one dimer of the octameric *M. tuberculosis* NadE is shown without transparency for comparison with *B. thailandensis*. *D*, schematic organization of the NAD synthetase domain N and the glutaminase domain G in the dimeric and in the octameric conformation of NadE^{Gln}. Note that the relative orientations between the N and G domains remain the same though through a domain-swap interaction in the octameric case. The PDB structures 4FH4 and 3DLA were visualized using PyMOL.

obtained by the Burkholderia structome project (21), we used this protein to analyze the structural features of the subgroup of dimeric NadE2^{Gln}. Structural alignments with other available NadE^{Gln} structures revealed that *B. thailandensis* is highly related to the dimeric NadE2^{Gln} from *A. baumannii* (data not shown) as anticipated by their degree of phylogenetic relationship (Fig. 4), hence supporting that *B. thailandensis* NadE2^{Gln} may serve as a prototype for this group of enzymes. Alignments with NAD synthetase NadE^{NH3} from *Bacillus subtilis* (22) revealed structural conservation at the NAD synthetase domain structures (Fig. S5).

Comparison between the dimeric *B. thailandensis* NadE2 and the octameric *M. tuberculosis* NadE1 (13) revealed that the individual domains are structurally very similar with conserved residues involved in substrate binding and domain folding (Fig. 1). However, they display a rearrangement of the relative domain positions within the protomers (Fig. 5). In *B. thailandensis* NadE2, the glutaminase and synthetase domains within the same polypeptide make extensive contacts and are located in the same plane (Fig. 5, *A–C*). On the other hand, in the case of *M. tuberculosis* NadE1, the glutaminase domain of one polypeptide extends to make contact with the NaAD sythetase domain of the next polypeptide in the octamer through a flexible loop comprising resides 313–331 (MtNadE1^{Gln} numbering) (Fig. 5, *A–C*). This particular segment is shorter in the dimeric subgroup of proteins (Fig. 1). This flexible loop facilitates the extensive intersubunit contacts in the octameric structure of *M. tuberculosis*. The superimposed picture of the two structures (Fig. 5*A*) shows how the glutaminase domain of *M. tuberculosis* translates by ~40 Å compared with the same domain in *B. thailandensis* and makes most of the surface contact with the next chain, which suggests that the glutaminase and the NaAD sythetase function of the domain likely occur within domains of two different polypeptides. This arrangement indicates that the relative orientations between the N and G domains remain the same though through a domain-swap interaction in the octameric case (Fig. 5*D*). This is illustrated by the high structural similarity of the dimeric protein to the octameric when allowing for structural superpositions over different monomers. In this case the dimeric (PDB code 4F4H) structure can be superposed on the octameric (PDB code 3DLA) structure with an RMSD of 1.85 Å over 741 aligned residues (*i.e.* superposing the boxed domains in Fig. 5*D*).

Surface representation of *B. thailandensis* NadE2^{Gln} showed that the conserved residues forming the glutaminase catalytic triad and the intersubunit NaAD–ATP bind sites are located in solvent-exposed pores (Fig. 6, *A* and *B*). A phosphate is present in the NaAD binding site of *B. thailandensis* NadE (not shown) and makes similar contacts as observed for the NaAD phosphates in the *M. tuberculosis* NadE structure (residues Asn-471 and Lys-635, *Mt* numbering) (23), hence suggesting similar substrate binding modes between octameric and dimeric NadE^{Gln} enzymes.

Given that the NaAD- and glutamine-binding sites are separated 40–50 Å in space (within the same protomer or between the two different promoters), we hypothesized that *B. thailandensis* NadE2^{Gln} should have an internal tunnel to translocate ammonia between the two catalytic domains as observed in MtNadE1^{Gln}. We used CAVER to search for internal tunnels within the *B. thailandensis* NadE2^{Gln} structure. This analysis identified two continuous tunnels that are potential routes for ammonia translocation. A 57.6 Å tunnel connects the glutaminase site from one promoter to the synthetase site in the other promoter (Fig. 6*C*). Another 58.3 Å tunnel connects the two catalytic domains within the same protomer (Fig. 6*D*). The interprotomer tunnel is U-shaped resembling the ammonia tunnel identified in the *M. tuberculosis* NadE, whereas the intrasubunit tunnel is Z-shaped (Fig. 6). Considering the protein symmetry, there are actually four possible pathways for ammonia translocation (G1 to S1, G1 to S2, G2 to S1, and G2 to S2); all these routes are interconnected by a major empty space located within the interprotomer/interdomain interface (Fig. 6).

A major bottleneck constriction (0.94 Å) in the ammonia tunnel is formed just after the glutaminase catalytic triad (Fig. 6, *E* and *F*). Given that the ammonia van der Waals radius is ~1.6 Å (24), it is likely that BtNadE2^{Gln} must go through conformational changes to allow ammonia transfer between the two cat-

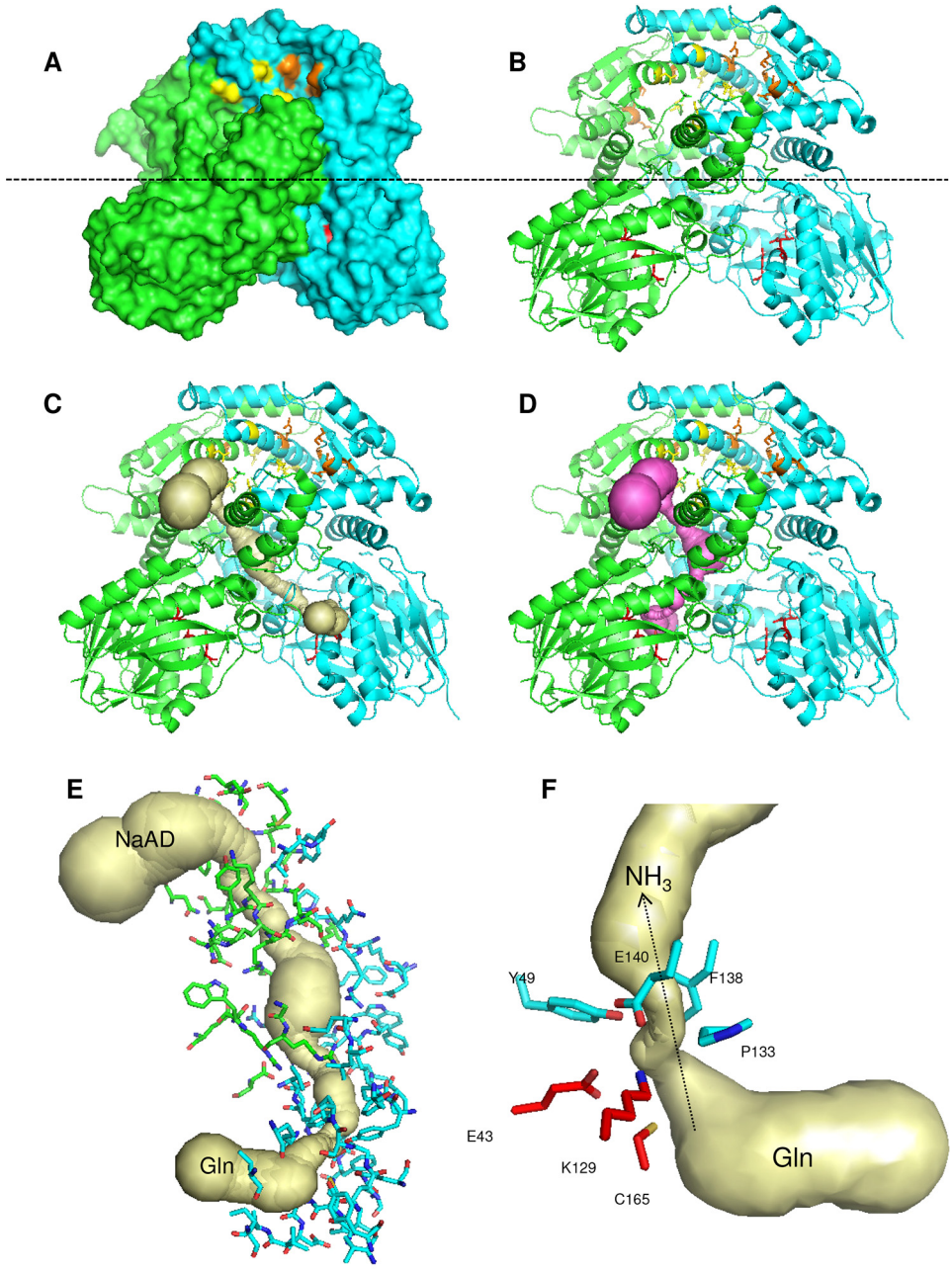

Figure 6. Structure of the dimeric NadE2^{Gln} from *B. thailandensis*. *A* and *B*, surface (*A*) and cartoon (*B*) representations; the monomers are colored *green* and *cyan*. The glutaminase catalytic triade residues are in *red sticks*. Residues involved in NaAD and ATP binding are shown as *yellow* and *orange sticks*, respectively. The *dashed line* indicates the separation of the NAD synthetase domain on the *top* and the glutaminase domain on the *bottom*. *C* and *D*, the ammonia tunnel connecting the glutaminase and NaAD synthetase domain in different protomers (*C*) and within the same protomer (*D*). The detailed structure of the intersubunit ammonia tunnel of the dimeric NadE2^{Gln} from *B. thailandensis* is shown. *E*, residues forming the intersubunit ammonia tunnel from different promoters are indicated as *green* and *cyan sticks*, respectively. *F*, conserved residues forming the major constriction within the ammonia tunnel are show in *cyan*, and the glutaminase catalytic residues are in *red*. The figures were generated using PyMOL and the PDB entry 4F4H. The ammonia tunnel was identified by CAVER.

alytic domains. The bottleneck constriction is mostly hydrophobic and formed by residues that are conserved in both octameric and dimeric forms of NadE^{Gln} (Figs. 1 and 6). The hydrophobic nature of the constriction suggests that ammonia rather than ionic ammonium may be the translocated species. A hydrophobic ammonia bottleneck or gate is also present in other ammonia-translocating proteins such as AmtB and GlmS (24, 25). In AmtB, conserved amino acid residues help to deprotonate ammonium before translacation (25), an important step to drive the equilibrium toward NH_3 formation under physiological pH considering the NH_4^+ pK_a of 9.2. More studies will be necessary to determine the nature of the translocated species in NadE2^{Gln}.

Discussion

In a previous study we reported the characterization of a NadE1^{Gln} from *H. seropedicae*, HsNadE1^{Gln}. We found that HsNadE1^{Gln} oligomerization and biochemical properties resemble the characteristics reported for the intensively studied MtNadE1^{Gln} and the *S. cerevisiae* NadE1^{Gln}. Here we report

the characterization of a second type of NadE2^{Gln} encoded by the genome of *H. seropedicae*, HsNadE2^{Gln}. Surprisingly, we found that HsNadE2^{Gln} is arranged in a completely novel oligomeric state (Fig. 2). Even though the experimentally determined molecular mass for HsNadE2^{Gln} was 85 kDa (which is between a monomer and dimer), it is more likely that HsNadE2^{Gln} is arranged as a dimer based on the phylogenetic relationship with other dimeric NadE2^{Gln} synthetases (Fig. 4).

Additional studies in *A. brasilense* revealed that this organism also encodes a dimeric form of NadE2^{Gln}, AbNadE2^{Gln} (Fig. 2). Further inspection in the PDB revealed the presence of dimeric NadE2^{Gln} in *A. baumannii* and *B. thailandensis*. These data suggest the presence of a novel group of dimeric NadE2^{Gln}. Phylogenetic analysis of NadE^{Gln} sequences from various organisms with diverse lifestyles support the presence two distinct groups of NadE^{Gln} in prokaryotes (Fig. 4). It is tempting to speculate that the group containing MtNadE1^{Gln}, AbNadE1^{Gln}, and HsNadE1^{Gln} (all octameric), is likely to be formed mostly by octameric types of NadE1^{Gln}, whereas the group containing HsNadE2^{Gln}, AbNadE2^{Gln}, *A. baumannii* NadE2^{Gln}, and *B. thailandensis* NadE2^{Gln} (all dimeric) should be mostly composed of dimeric forms of NadE2^{Gln}.

Structural analysis of *B. thailandensis* dimeric NadE2^{Gln} showed that this enzyme shares some features with octameric MtNadE1^{Gln}: the residues involved in substrate binding and catalysis and the residues forming a long intersubunit tunnel that are likely to carry ammonia from the glutaminase to the synthetase domain (Figs. 1 and 6). However, although BtNadE2^{Gln} has an intensive intrachain glutaminase-synthetase domain contact, such contacts are virtually absent in the MtNadE1^{Gln} enzyme (Fig. 5). The octameric NadE1^{Gln}-like forms presumably evolved to make much more intersubunit contacts, a property that may explain the strong domain synergism detected in MtNadE1^{Gln} (13) and the little efficiency of NadE1^{Gln}-like in using ammonium as N source (Tables 1 and 2).

The sequences of deep branching Bacteria (Thermotoga and Aquifex) and Archaea cluster in the NadE2^{Gln}-like dimeric group (Fig. 4). A previous phylogentic analysis suggested that a single-domain NadE^{NH3} was present in last universal common ancestor and the two-domain NadE^{Gln} evolved via recruitment and fusion of the N-terminal glutaminase domain (9). If this assumption is correct, we speculate that the dimeric NadE2^{Gln} could be an intermediate evolutionary link between the single-domain dimeric NadE^{NH3} and two domain octameric NadE1^{Gln}. Indeed, the enzymatic characteristics of the NadE2^{Gln} enzymes (Tables 1 and 2) show intermediate properties between dimeric NadE^{NH3} and octameric NadE1^{Gln} (*i.e.* NadE2^{Gln} can use both ammonium and glutamine with similar efficiencies). The biogeochemical history of earth support that although ammonium was readily available to the ancient life forms (that could support NadE^{NH3} activity), ammonium is very limited in most habitats nowadays, and this could explain the need to recruit a glutaminase domain to support NadE function during evolution.

More than one copy of NadE has been detected in the genome of a range of prokaryotes (see Table S3 in Ref. 9). One intriguing question remaining to be answered is why some

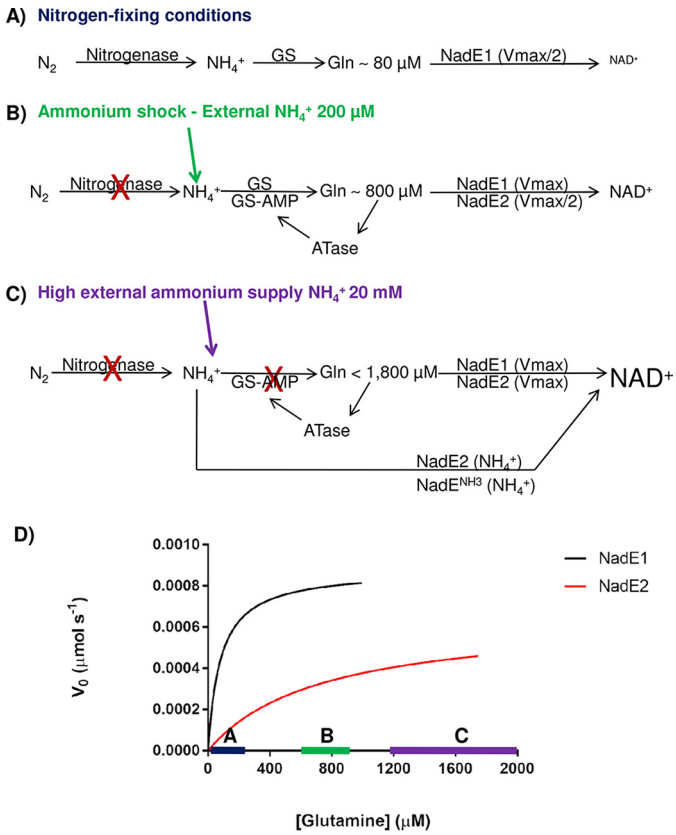

Figure 7. Model for the role of the three NadE in *A. brasilense*. *A*, under nitrogen-fixing conditions nitrogenase feeds ammonium into GS, and intracellular levels of glutamine are low (~80 μM). NadE1^{Gln} operates at V_{max}/2 and promptly responds to small fluctuations in glutamine availability within this range (see the *blue bar* with Michaelis–Menten curves in *D*). NadE2^{Gln} and NadE^{NH3} activities are negligible leading to slow production of NAD$^+$. *B*, upon an ammonium shock of NH_4^+ 200 μM, the intracellular glutamine rises to ~800 μM, leading to total inhibition of nitrogenase by ADP-ribosylation and nearly full inhibition of GS by adenylylation. NadE1^{Gln} operates at V_{max}, whereas NadE2^{Gln} operates at V_{max}/2 and promptly responds to small fluctuations in glutamine availability within this range (see the *green bar* with Michaelis–Menten curves in *D*). NAD$^+$ production is elevated. *C*, when external levels of ammonium are high, the high intracellular glutamine will lead to NadE1^{Gln} and NadE2^{Gln} to operate at V_{max} using glutamine as substrate. Furthermore, because GS is fully inactive due adenylylation, free intracellular ammonium could be directly assimilated into NAD$^+$ by NadE2^{Gln} and presumably also by NadE^{NH3} bypassing GS activity. The concert action of all three isoforms of NadE is likely to further enhance NAD$^+$ production. *D*, velocities of the different *A. brasilense* NadE isoforms accordingly to the intracellular glutamine levels.

organisms encode multiple isoforms of NadE. Different expression in response to nitrogen availability would be one possible explanation; however, at least in the case of *A. brasilense,* proteomic analysis revealed that AbNadE1^{Gln}, AbNadE2^{Gln}, and AbNadE^{NH3} levels did not change in response to ammonium availability.[3] Hence, the different kinetic properties and/or substrate preferences may constitute the only selective pressure to maintain three NadE isoforms within the *A. brasilense* genome. Our data allowed us to propose a model for the role of these isoforms in *A. brasilense*. Under nitrogen-fixing conditions, the intracellular levels of glutamine are low (~80 μM), and NadE1^{Gln} operates at V_{max}/2 and thereby prompts responses to small fluctuations in glutamine availability within this range accordingly to the NadE1 Michaelis–Menten curve (Fig. 7, *A*

[3] C. Kukolj and Souza EM, personal communication.

and *D*). Upon an ammonium shock of NH_4^+ 200 μM, the intracellular glutamine raises to ~800 μM, NadE1 operates at V_{max}, whereas NadE2^{Gln} operates at $V_{max}/2$ and thereby prompts responses to small fluctuations in glutamine availability within this range (Fig. 7, *B* and *D*). Hence, the presence of two glutamine-dependent NadEs would allow better adjustment of NAD^+ production over a broad range of glutamine concentrations (Fig. 7).

We did not measure the intracellular glutamine concentrations under a high ammonium regime; however, in *E. coli* concentrations of 1.9–5 mM under high ammonium regime were detected (26–28). When *A. brasilense* receives an ammonium shock of 20 mM NH_4Cl, GS is fully adenylylated and inactive after 2 min.[4] If we assume that intracellular ammonium levels could be similar to external levels because of ammonia diffusion through the cytoplasmic membrane (29) and lack of active GS under 20 mM NH_4Cl, then NadE2^{Gln} (and presumably also NadE^{NH3}) could bypass GS and directly assimilate ammonium into NAD^+ (Fig. 7*C*).

The presence of NadE isoforms that are able to bypass GS under high ammonium regimes would be energetic advantageous giving that GS activity may consume up to 15% of the cellular ATP (30). Energy saving may be particularly important in dynamic and competitive niches such as soil and rhizosphere, the habitats were *A. brasilense* is found.

Experimental procedures

Plasmid construction

Isolation of plasmid DNA, gel electrophoresis, bacterial transformation, and cloning were performed using standard protocols. T4 DNA ligase and the restriction enzymes NdeI and BamHI were purchase from Fermentas and were used following the manufacturers' instructions. The genes *nadE2* from *H. seropedicae* SMR1, *nadE1*, *nadE2*, and *nadE3* from *A. brasilense* FP2 were amplified by PCR using DNA from boiled culture as template and high-fidelity polymerase *Pfu* (Fermentas). PCR fragments and expression vectors pET28a, pET29a, and pTEV5 were digested with NdeI and BamHI and ligated. The primers used in PCR are listed on Table S1. DNA sequencing was performed using dye-labeled terminators (BigDye® ABI PRISM) in an automated DNA sequencer ABI 3500 from Applied Biosystems. Recombinant plasmids obtained in this work were: pASnade2 (Express *H. seropedicae* NadE2^{Gln} with a N-terminal His_6 tag in pET28a), pASnade3 (Express *A. brasilense* NadE^{NH3} with a N-terminal His_6 tag in pTEV5), pLHnade2 (Express native *A. brasilense* NadE2^{Gln} in pET29a), and pASnade1 (Express *A. brasilense* NadE1 with a N-terminal His_6 tag in pTEV5).

Protein purification

NadE proteins were overexpressed in freshly transformed *E. coli* BL21 (λDE3) and purified adapting previous protocols (12). Typically, the cells were grown in LB medium to an $A_{600\,nm}$ of 0.7 at 37 °C. The incubation temperature was changed to 16 °C, and protein expression was induced by adding 0.5 mM isopropyl β-D-thiogalactopyranoside. The cells were harvested after 12 h of shaking at 200 rpm. For His-tagged protein purification (AbNadE1^{Gln}, AbNadE^{NH3}, HsNadE1^{Gln}, and HsNadE2^{Gln}), the cell pellets from 0.8 liter of culture were resuspended in 40 ml of buffer A: 50 mM Tris-HCl, pH 8.0, 100 mM NaCl, 20% (v/v) glycerol. The cells were lysed by sonication and centrifuged. The soluble fraction used for His-NadE purification using Ni^{2+} affinity chromatography on a Hi-trap chelating column (GE Healthcare); the proteins were eluted using a imidazole gradient. Protein concentration was measured at 595 nm by Bradford reaction assay (Bio-Rad).

When indicated, TEV protease was used to remove the N-terminal His_6 tag fusion as follows: purified AbNadE1^{Gln} and AbNadE^{NH3} proteins were mixed with His-TEV protease at a 9:1 ratio in 50 mM Tris-HCl, pH 8, 100 mM NaCl, 1 mM DTT. The mixture was incubated at 8 °C for 20 h. His-TEV and uncleaved NadE protein were removed using a Ni^{2+} Hi-trap chelating column (GE Healthcare). Cleavage was verified by SDS-PAGE electrophoresis. The final preparation has four additional residues (Gly–Ala–Ser–His) at the N terminus of the TEV protease cleavage site.

The *A. brasilense* NadE2^{Gln} was purified without tags. The plasmid pLHnadE2 was used to express untagged NadE2^{Gln} in *E. coli* BL21 (λDE3) as described above. The cell pellet was resuspended in buffer A (50 mM Tris-HCl, pH 8.0, 100 mM NaCl, 20% (v/v) glycerol) and sonicated. The soluble fraction was loaded onto a Q-Sepharose column, and proteins were eluted with 0.1–1 M linear gradient of NaCl. Fractions containing NadE were pooled and loaded onto a gel filtration HiLoad Superdex 200 16/60 column (GE Healthcare).

Gel filtration and MW determination

Analytical size-exclusion chromatography was performed in a 24-ml Superose 6 column (GE Healthcare) using 50 mM Tris-HCl, pH 8, and 100 mM NaCl as buffer. The column was calibrated with the molecular weight standards: thyroglobulin, bovine γ-globulin, chicken ovalbumin, and equine myoglobin (Bio-Rad). The log of molecular weight was plotted against the K_{av} (partition coefficient of each standard) to build a linear calibration curve. The molecular weight of each protein was determined by comparing the K_{av} against the calibration curve.

NadE kinetic analysis

The NadE activity was monitored by coupling the NAD^+ production to its reduction to NADH using alcohol dehydrogenase from yeast (Sigma) and monitoring NADH formation at 340 nm as described previously (12). The assays were carried out at 30 °C in 62 mM Tris-HCl, pH 8.5, 20 mM KCl, 20 mM $MgCl_2$, 1.6% (v/v) ethanol, 10 mM DTT, 6 units of yeast alcohol dehydrogenase (Sigma) and 50 nM of NadE (monomer concentration). To determine the kinetic constants, the substrates ATP and NaAD were kept at saturating concentrations (10 and 1 mM, respectively), whereas glutamine or ammonium (NH_4Cl) varied from 2.5 to 10,000 μM and from 50 to 100,000 μM, respectively. The assays were performed in triplicate, and the initial velocity data were fitted to the Michaelis–Menten equation using GraphPad Prism software package.

[4] L. F. Huergo, unpublished observations.

LC/MS analysis ammonium versus glutamine substrate competition

Competition assays were performed combining different amounts of glutamine and ^{15}N-labeled NH_4Cl (Sigma). Reactions containing the two substrates were performed in 20 mM Tris-HCl, pH 8, 2 mM ATP, 2 mM NaAD, 5 mM $MgCl_2$, and 1 mM DTT. The reactions were started by adding 50 nM of NadE (monomer concentration) and incubated at 30 °C for 5 min. Acetic acid to 10% (v/v) was added to quench the reactions. The samples were centrifuged at 20,000 × *g* for 5 min at 4 °C, and 10 μl of the supernatant was used for LC/MS analysis as described (31). Metabolites were separated using a UFLC Prominence (Shimadzu) in a C18 column of 2.6 μm and 50 × 2.1 mm (Phenomenex) kept at 40 °C. The mobile phases were composed of 15 mM acetic acid and 10 mM tributylamine (solvent A) or methanol (solvent B). Samples were placed into vials and kept in an auto-sampler at 4 °C; 10 μl of each sample was injected at 0.2 ml min^{-1} in duplicate. Metabolites were eluted from the column using a linear gradient (0–100% of solvent B) in 30 min. The detection of the metabolites was performed by coupling the LC with a MicroTOF-QII (Bruker Daltonics), equipped with an electrospray ionization source. The retention time of NAD^+ was confirmed using a standard solution.

The ^{15}N incorporation was determined by the formula: intensity peak *m*/*z* 663 − (0.227 × intensity peak *m*/*z* 662). This value represents the increase in the *m*/*z* 663.1 signal because of ^{15}N ammonium incorporation subtracted from the theoretical 22.7% isotopic contribution of 1-[^{13}C-^{14}N]NAD^+). The value obtained (which corresponds only to [^{12}C-^{15}N]NAD^+) was divided by the signal of [^{14}N]glutamine incorporation at 662 *m*/*z* to give the ^{15}N NH_4^+/[^{14}N]Gln incorporation ratio.

Intracellular levels of glutamine and protein post-translational modification analysis

A. brasilense FP2 was cultured in 110 ml of NfbHP medium containing 5 mM glutamate as nitrogen source, and nitrogenase activity was determined by the acetylene reduction method using GC exactly as described previously (18). The *A. brasilense* cells were subjected to an ammonium shock (NH_4Cl 200 μM) while being kept in a rotatory shaker incubator at 120 rpm and 30 °C. The samples were collected at −5, 0, 0.5, 1, 2, 5, 10, and 20 min after ammonium addition. To analyze the effectiveness of the ammonium shock, the post-translational modification of the GS and NifH proteins were monitored by Western blotting exactly as described previously (18).

For the extraction of metabolites, 2-ml samples were rapidly collected and quickly cooled in liquid nitrogen. The samples were centrifuged for 2 min at 20,000 × *g* at 4 °C, and the cell pellets were resuspended in 60 μl of ice-cold solvent (40:40:20 acetonitrile:methanol:water and 0.1 M formic acid) and kept for 20 min at −20 °C as described (26). The extracts were centrifuged at 20,000 × *g* at 4 °C for 3 min, the supernatant was transferred to a new tube, and the pellet was subjected to another round of metabolite extraction. The supernatant from the two extractions were combined and neutralized with 4 μl of ammonium hydroxide. The samples were centrifuged (20,000 × *g*, 20 min, 4 °C), and supernatant was subject to LC/MS analysis.

Separation and detection of metabolites was performed using a LC/MS equipment as described for NadE glutamine *versus* ammonium completion assays (see above). The high resolution MicroTOF-QII (Bruker Daltonics) was set to an acquisition interval of 50–1000 *m*/*z* and sampling rate of 1 s operating on negative MS mode. The capillary voltage was maintained at 3,500 V, and end-plate offset was −500 V. The nebulizer gas flow was 2.0 bar, and the dry gas was kept at 6.0 liters min^{-1} at 180 °C. All samples were subject to technical replicate runs. The equipment was calibrated with a standard curve of glutamine ($R^2 > 0.98$) before each analysis. All samples were analyzed within the linear range of the calibration curve. The data were processed using QuantiAnalysis (version 4.0 SP1 Bruker). The metabolites were extracted using calculated *m*/*z* with an error window of ± 0.01 *m*/*z*, and retentions times were confirmed by comparison with standards.

To calculate intracellular glutamine concentrations, the number of viable cells in each experiment was counted by serial dilution plating. Metabolite intracellular concentration was calculated based on the number of cells and the estimated intracellular volume of *A. brasilense* of 2.35 μm^3 (1-μm diameter × 3-μm length).

Author contributions—A. R. S. S., E. C. M. G., F. O. P., E. M. S., M. H., and L. F. H. conceptualization; A. R. S. S., E. C. M. G., V. R. M., R. D., M. H., and L. F. H. data curation; A. R. S. S., E. C. M. G., R. D., and M. H. formal analysis; A. R. S. S., E. C. M. G., and L. F. H. investigation; A. R. S. S., E. C. M. G., V. R. M., and L. F. H. methodology; E. C. M. G., V. R. M., and L. F. H. supervision; F. O. P., E. M. S., and L. F. H. funding acquisition; F. O. P., E. M. S., and L. F. H. project administration; R. D. writing-review and editing; M. H. and L. F. H. writing-original draft; L. F. H. software.

References

1. Li, J., Bonkowski, M. S., Moniot, S., Zhang, D., Hubbard, B. P., Ling, A. J., Rajman, L. A., Qin, B., Lou, Z., Gorbunova, V., Aravind, L., Steegborn, C., and Sinclair, D. A. (2017) A conserved NAD^+ binding pocket that regulates protein–protein interactions during aging. *Science* **355,** 1312–1317 CrossRef Medline
2. Moure, V. R., Costa, F. F., Cruz, L. M., Pedrosa, F. O., Souza, E. M., Li, X. D., Winkler, F., and Huergo, L. F. (2015) Regulation of nitrogenase by reversible mono-ADP-ribosylation. *Curr. Top. Microbiol. Immunol.* **384,** 89–106 Medline
3. Aravind, L., Zhang, D., de Souza, R. F., Anand, S., and Iyer, L. M. (2015) The natural history of ADP-ribosyltransferases and the ADP-ribosylation system. *Curr. Top. Microbiol. Immunol.* **384,** 3–32 Medline
4. Bheda, P., Jing, H., Wolberger, C., and Lin, H. (2016) The substrate specificity of sirtuins. *Annu. Rev. Biochem.* **85,** 405–429 CrossRef Medline
5. Gazzaniga, F., Stebbins, R., Chang, S. Z., McPeek, M. A., and Brenner, C. (2009) Microbial NAD metabolism: lessons from comparative genomics. *Microbiol. Mol. Biol. Rev.* **73,** 529–541 CrossRef Medline
6. Brenner, C. (2002) Catalysis in the nitrilase superfamily. *Curr. Opin. Struct. Biol.* **12,** 775–782 CrossRef Medline
7. Rizzi, M., Nessi, C., Mattevi, A., Coda, A., Bolognesi, M., and Galizzi, A. (1996) Crystal structure of NH_3-dependent NAD^+ synthetase from *Bacillus subtilis*. *EMBO J.* **15,** 5125–5134 Medline
8. Jauch, R., Humm, A., Huber, R., and Wahl, M. C. (2005) Structures of *Escherichia coli* NAD synthetase with substrates and products reveal mechanistic rearrangements. *J. Biol. Chem.* **280,** 15131–15140 CrossRef Medline

9. de Ingeniis, J., Kazanov, M. D., Shatalin, K., Gelfand, M. S., Osterman, A. L., and Sorci, L. (2012) Glutamine versus ammonia utilization in the NAD synthetase family. *PLoS One* **7,** e39115 CrossRef Medline
10. Bellinzoni, M., De Rossi, E., Branzoni, M., Milano, A., Peverali, F. A., Rizzi, M., and Riccardi, G. (2002) Heterologous expression, purification, and enzymatic activity of *Mycobacterium tuberculosis* NAD^+ synthetase. *Protein. Expr. Purif.* **25,** 547–557 CrossRef Medline
11. Resto, M., Yaffe, J., and Gerratana, B. (2009) An ancestral glutamine-dependent NAD^+ synthetase revealed by poor kinetic synergism. *Biochim. Biophys. Acta* **1794,** 1648–1653 CrossRef Medline
12. Laskoski, K., Santos, A. R., Bonatto, A. C., Pedrosa, F. O., Souza, E. M., and Huergo, L. F. (2016) *In vitro* characterization of the NAD^+ synthetase NadE1 from *Herbaspirillum seropedicae*. *Arch. Microbiol.* **198,** 307–313 CrossRef Medline
13. LaRonde-LeBlanc, N., Resto, M., and Gerratana, B. (2009) Regulation of active site coupling in glutamine-dependent NAD^+ synthetase. *Nat. Struct. Mol. Biol.* **16,** 421–429 CrossRef Medline
14. van Heeswijk, W. C., Westerhoff, H. V., and Boogerd, F. C. (2013) Nitrogen assimilation in *Escherichia coli*: putting molecular data into a systems perspective. *Microbiol. Mol. Biol. Rev.* **77,** 628–695 CrossRef Medline
15. Huergo, L. F., and Dixon, R. (2015) The emergence of 2-oxoglutarate as a master regulator metabolite. *Microbiol. Mol. Biol. Rev.* **79,** 419–435 CrossRef Medline
16. Huergo, L. F., Pedrosa, F. O., Muller-Santos, M., Chubatsu, L. S., Monteiro, R. A., Merrick, M., and Souza, E. M. (2012) PII signal transduction proteins: pivotal players in post-translational control of nitrogenase activity. *Microbiology* **158,** 176–190 CrossRef Medline
17. Dixon, R., and Kahn, D. (2004) Genetic regulation of biological nitrogen fixation. *Nat. Rev. Microbiol.* **2,** 621–631 CrossRef Medline
18. Huergo, L. F., Souza, E. M., Araujo, M. S., Pedrosa, F. O., Chubatsu, L. S., Steffens, M. B., and Merrick, M. (2006) ADP-ribosylation of dinitrogenase reductase in *Azospirillum brasilense* is regulated by AmtB-dependent membrane sequestration of DraG. *Mol. Microbiol.* **59,** 326–337 CrossRef Medline
19. Huergo, L. F., Chandra, G., and Merrick, M. (2013) P(II) signal transduction proteins: nitrogen regulation and beyond. *FEMS Microbiol. Rev.* **37,** 251–283 CrossRef Medline
20. Tautenhahn, R., Patti, G. J., Rinehart, D., and Siuzdak, G. (2012) XCMS Online: a web-based platform to process untargeted metabolomic data. *Anal. Chem.* **84,** 5035–5039 CrossRef Medline
21. Baugh, L., Gallagher, L. A., Patrapuvich, R., Clifton, M. C., Gardberg, A. S., Edwards, T. E., Armour, B., Begley, D. W., Dieterich, S. H., Dranow, D. M., Abendroth, J., Fairman, J. W., Fox, D., 3rd, Staker, B. L., Phan, I., *et al.* (2013) Combining functional and structural genomics to sample the essential Burkholderia structome. *PLoS One* **8,** e53851 CrossRef Medline
22. Symersky, J., Devedjiev, Y., Moore, K., Brouillette, C., and DeLucas, L. (2002) NH_3-dependent NAD^+ synthetase from *Bacillus subtilis* at 1A resolution. *Acta Crystallogr. D Biol. Crystallogr.* **58,** 1138–1146 CrossRef Medline
23. Chuenchor, W., Doukov, T. I., Resto, M., Chang, A., and Gerratana, B. (2012) Regulation of the inter subunit ammonia tunnel in *Mycobacterium tuberculosis* glutamine-dependent NAD^+ synthetase. *Biochem. J.* **443,** 417–426 CrossRef Medline
24. Floquet, N., Mouilleron, S., Daher, R., Maigret, B., Badet, B., and Badet-Denisot, M. A. (2007) Ammonia channeling in bacterial glucosamine-6-phosphate synthase (Glms): molecular dynamics simulations and kinetic studies of protein mutants. *FEBS Lett.* **581,** 2981–2987 CrossRef Medline
25. Javelle, A., Lupo, D., Ripoche, P., Fulford, T., Merrick, M., and Winkler, F. K. (2008) Substrate binding, deprotonation, and, selectivity at the periplasmic entrance of the *Escherichia coli* ammonia channel AmtB. *Proc. Natl. Acad. Sci. U.S.A.* **105,** 5040–5045 CrossRef Medline
26. Bennett, B. D., Kimball, E. H., Gao, M., Osterhout, R., Van Dien, S. J., and Rabinowitz, J. D. (2009) Absolute metabolite concentrations and implied enzyme active site occupancy in *Escherichia coli*. *Nat. Chem. Biol.* **5,** 593–599 CrossRef Medline
27. Yuan, J., Doucette, C. D., Fowler, W. U., Feng, X. J., Piazza, M., Rabitz, H. A., Wingreen, N. S., and Rabinowitz, J. D. (2009) Metabolomics-driven quantitative analysis of ammonia assimilation in *E. coli*. *Mol. Syst. Biol.* **5,** 302 Medline
28. Okano, H., Hwa, T., Lenz, P., and Yan, D. (2010) Reversible adenylylation of glutamine synthetase is dynamically counterbalanced during steady-state growth of *Escherichia coli*. *J. Mol. Biol.* **404,** 522–536 CrossRef Medline
29. Kleiner, D. (1985) Bacterial ammonium transport. *FEMS Microbiol. Lett.* **32,** 87–100 CrossRef
30. Reitzer, L. (2003) Nitrogen assimilation and global regulation in *Escherichia coli*. *Annu. Rev. Microbiol.* **57,** 155–176 CrossRef Medline
31. Rodrigues, T. E., Gerhardt, E. C., Oliveira, M. A., Chubatsu, L. S., Pedrosa, F. O., Souza, E. M., Souza, G. A., Müller-Santos, M., and Huergo, L. F. (2014) Search for novel targets of the PII signal transduction protein in Bacteria identifies the BCCP component of acetyl-CoA carboxylase as a PII binding partner. *Mol. Microbiol.* **91,** 751–761 CrossRef Medline